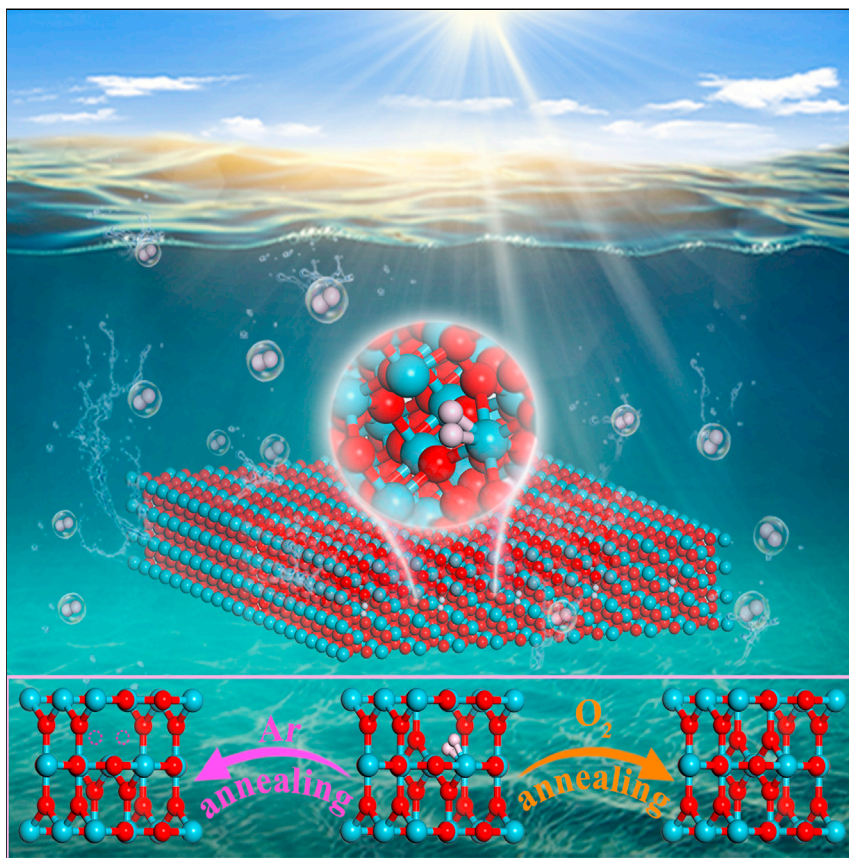


Article

Wet-chemistry hydrogen doped TiO₂ with switchable defects control for photocatalytic hydrogen evolution



Hydrogenated TiO₂ (H-TiO₂) has been verified as a promising photocatalytic material. The conventional H-TiO₂ is mainly prepared by posttreatment. A new wet-chemistry strategy is developed by synthesizing a hydrogenated TiO₂ by one-step chemical method in alcoholic solution. The H-TiO₂ shows a 60-fold improvement compared with commercial rutile. Also, the H-TiO₂ exhibits unprecedented defects engineering ability, that is, TiO₂ with or without oxygen vacancies could be separately obtained by annealing in Ar or O₂ atmosphere, respectively.

Guangri Jia, Ying Wang,
Xiaoqiang Cui, ..., Weiwei Li, Lei
Zhang, Weitao Zheng

xqcui@jlu.edu.cn

Highlights

The H-TiO₂ is synthesized by a new one-step wet-chemistry approach

H-TiO₂ can yield switchable defect via controlled annealing atmosphere

H-TiO₂ exhibits the enhanced photocatalytic property over commercial rutile and P25

Development

Practical, real world, technological considerations and constraints

6

Jia et al., Matter 5, 206–218
January 5, 2022 © 2021 Elsevier Inc.
<https://doi.org/10.1016/j.matt.2021.10.027>



Article

Wet-chemistry hydrogen doped TiO₂ with switchable defects control for photocatalytic hydrogen evolution

Guangri Jia,^{1,9} Ying Wang,^{1,9} Xiaoqiang Cui,^{1,10,*} Hengzhong Zhang,² Jingxiang Zhao,³ Lu Hua Li,⁴ Lin Gu,⁵ Qinghua Zhang,⁵ Lirong Zheng,⁶ Jiandong Wu,¹ Qiong Wu,¹ David J. Singh,⁷ Weiwei Li,² Lei Zhang,^{1,8} and Weitao Zheng¹

HPSTAR
1360-2022

SUMMARY

Hydrogen has a remarkably flexible chemistry in oxides. We show that the introduction of H into simple TiO₂ leads to greatly enhanced photocatalytic properties, and specifically yields a 60 times enhancement of photocatalytic hydrogen evolution activity over commercial rutile. The hydrogenated TiO₂ (H-TiO₂) is synthesized by a new one-step wet-chemistry approach yielding switchable defect via controlled annealing. As-prepared H-TiO₂ has Ti-H bonds in the lattice from replacement of oxygen by hydrogen atoms. The Ti-H bonds are converted to oxygen vacancies by loss of H₂O with Ar annealing. Oppositely, Ti-H defects are healed by Ti-O with O₂ annealing. The strongly enhanced photocatalytic activity is associated with increased visible light absorption and effective separation of photogenerated carriers. This work provides a new and powerful approach for the preparation of hydrogenated titanium dioxide with switchable defect control, and striking improvement of photocatalytic activity.

INTRODUCTION

Defect engineering is a promising approach for enhancing photocatalytic performance of titanium dioxide.^{1–7} Specifically, hydrogenating TiO₂ (to form H-TiO₂) enhances the performance by (1) narrowing the TiO₂ band gap (3.2 eV),^{8–10} and (2) inhibiting carrier recombination.^{11–13} Hydrogenated TiO₂ is generally prepared by a two-step strategy of post-treating anatase TiO₂ nanostructures by harsh hydrogen reduction.^{14–20} For instance, hydrogenated black TiO₂ can be prepared in a 20.0-bar H₂ atmosphere at approximately 200°C for 5 days.² Red anatase TiO₂ photocatalysts with hydrogen-filled oxygen vacancies can be made at 360°C in a hydrogen atmosphere.¹⁶ H-doped TiO₂ can also be prepared by hydrogen plasma, MgH₂ reduction, and metal-acid treatment of TiO₂ nanoparticles.^{18,21,22} Developing more facile TiO₂ hydrogenation strategies using milder conditions to synthesize both rutile and anatase phase hydrogenated TiO₂ and controlling incorporation of switchable defects are essential for further enhancing catalytic performance and utility. This also poses a fascinating fundamental challenge, since the improved activity of H-TiO₂ relative to TiO₂ and the difficulty in hydrogenating TiO₂ are related to the chemistry of H in oxides, specifically the weaker bonding of anionic H in the lattice relative to O and the associated changes in the position of the orbitals of Ti adjacent to H.

Here, we present a new wet-chemistry method for *in situ* hydrogenation of TiO₂. Hydrogen atoms from alcohol dehydrogenation are incorporated into TiO₂ during

Progress and potential

The conversion of solar energy into solar fuel through photocatalytic water splitting is a promising means to solve energy and environmental problems. Recently, hydrogenated TiO₂ (H-TiO₂) has been verified as a promising photocatalytic material. H-TiO₂ is mainly prepared by posttreatment, such as high temperature reduction, hydrogen plasma, and metal hydride reduction and so on. It is essential to develop more facile H-TiO₂ strategies using milder conditions and controlling switchable defects for enhancing catalytic performance. Here, we present a new wet-chemistry method for H-TiO₂, which shows an excellent photocatalytic H₂ evolution activity by increasing light absorption, accelerating carrier effective separation, and reducing hydrogen adsorption free energy after H incorporation and yields switchable defect via controlled annealing. This finding offers a pathway for the preparation of efficient photocatalysts based on TiO₂ and illustrates a promising avenue for defect engineering in oxides.



the hydrolysis of tetrabutyl titanate in trifluoromethanesulfonic (TfOH) solution. Ti-H defects are formed in H-TiO₂ when hydrogen atoms replace oxygen atoms, while preserving the original TiO₂ crystal structure. Also, this method for synthesizing H-TiO₂ provides an unprecedented opportunity for switchable defect engineering: TiO₂ with or without oxygen vacancies can be controllably obtained by annealing in Ar or O₂ atmospheres, respectively. Furthermore, H-TiO₂ shows an enhanced photocatalytic hydrogen evolution activity, which is 60 times that of the commercial rutile (C-rutile). The H incorporation changes the band structure and extends visible light absorption by introducing bandgap states in TiO₂. The H defects change the charge distribution around Ti and O, promoting efficient separation of photocarriers. This work offers a pathway for the preparation of efficient photocatalysts based on TiO₂ and illustrates a promising avenue for defect engineering in oxides.

RESULTS AND DISCUSSION

Morphology and structural characterization

Preparation of H-TiO₂ nanostructures and subsequent switchable defect engineering are illustrated in **Figure 1A**. When TfOH is added in the solution of tetrabutyl (IV) titanate and alcohol, the hydrolysis product is H-TiO₂. Oppositely, the conventional anatase TiO₂ is obtained when water is used for hydrolysis. The Ti-H defects of H-TiO₂ can be switched into oxygen vacancies with Ar annealing, and conversely recovered into Ti-O with O₂ annealing. The ratio between added TfOH and H₂O plays an essential role for the products. X-ray diffraction (XRD) characterization shows that rutile H-TiO₂ was obtained with 100% TfOH, but anatase was obtained with 0% TfOH, i.e., 100% water (**Figures 1B** and **S1**). The morphology of products evolves from anatase nanoparticles to rutile nanorods when the concentration of TfOH increases from 0% to 100% based on the scanning electron microscopy and transmission electron microscope (TEM) images (**Figures S2** and **S3**). Along with the increased content of the organic acid, it is found that the TiO₂ changes from nanoparticles with sizes of 10.4 ± 0.1 nm (TiO₂-0%) and 8.8 ± 0.1 nm (TiO₂-50%) to nanorods with diameters from 17.8 ± 0.2 nm (TiO₂-95%) to 16.1 ± 0.1 nm (TiO₂-100%) (**Figures S4** and **S5**). The heterojunction structure with rutile and anatase phase TiO₂ was obtained in 75% TfOH (**Figure S6**). ¹H solid-state nuclear magnetic resonance (NMR) spectroscopy is used to investigate the incorporation of H into TiO₂.²³ An additional peak appears at 0.78 ppm (peak A) (**Figures 1C** and **S7**), which is attributed to the formation of bonds in H and Ti atoms.^{16,22} New peak at 2.6 ppm (peak B) is ascribed to the H inside the titanol group.^{18,22} The peak at 5.4 ppm (peak C) is assigned to the hydroxyl group from external water adsorption on the surface.¹⁶ These observations indicate that H-doped TiO₂ is synthesized and the structure of TiO₂ evolves in acidic condition.^{24,25} The participation of TfOH is essential for the formation of H-TiO₂. Ti-H moieties are formed *in situ* based on Lewis acid-base active center, which then serves as the active center for alcohol dehydrogenation in TfOH solution rather than water (**Figure S8**).^{26–28} The liquid Fourier transform infrared (FT-IR) test confirms the Ti-H is derived from alcohol dehydrogenation (**Figure S9**).²⁹

Importantly, the as-synthesized H-TiO₂ provides unprecedented possibilities of defects engineering. Thermogravimetric analysis shows different weight losses in N₂ and air atmospheres (**Figure 2A**). The first weight loss at 105°C is associated with the evaporation of the surface adsorbed water. The second stage has an obvious weight loss at 320°C in N₂. However, there is no weight loss at 320°C in air. Combined with the mass spectra, the weight loss at 320°C is because two hydrogen atoms leave the lattice and carry away one oxygen atom from the H-TiO₂ in N₂. Conversely, oxygen compensates for the loss of oxygen atoms in the lattice

¹State Key Laboratory of Automotive Simulation and Control, School of Materials Science and Engineering, and Key Laboratory of Automobile Materials of MOE, Jilin University, 2699 Qianjin Street, Changchun 130012, China

²Center for High Pressure Science and Technology Advanced Research, Shanghai 201203, China

³Key Laboratory of Photonic and Electronic Bandgap Materials, Ministry of Education, and College of Chemistry and Chemical Engineering, Harbin Normal University, Harbin 150025, China

⁴Institute for Frontier Materials, Deakin University, Geelong Waurn Ponds Campus, Waurn Ponds, VIC 3216, Australia

⁵Beijing National Laboratory for Condensed Matter Physics, Institute of Physics, Chinese Academy of Sciences, Beijing 100190, China

⁶Beijing Synchrotron Radiation Facility, Institute of High Energy Physics, Chinese Academy of Sciences, Beijing 100049, China

⁷Department of Physics and Astronomy and Department of Chemistry, University of Missouri, Columbia, MO 65211, USA

⁸College of Chemistry, Jilin University, 2699 Qianjin Street, Changchun 130012, China

⁹These authors contributed equally

¹⁰Lead contact

*Correspondence: xq cui@jlu.edu.cn

<https://doi.org/10.1016/j.matt.2021.10.027>

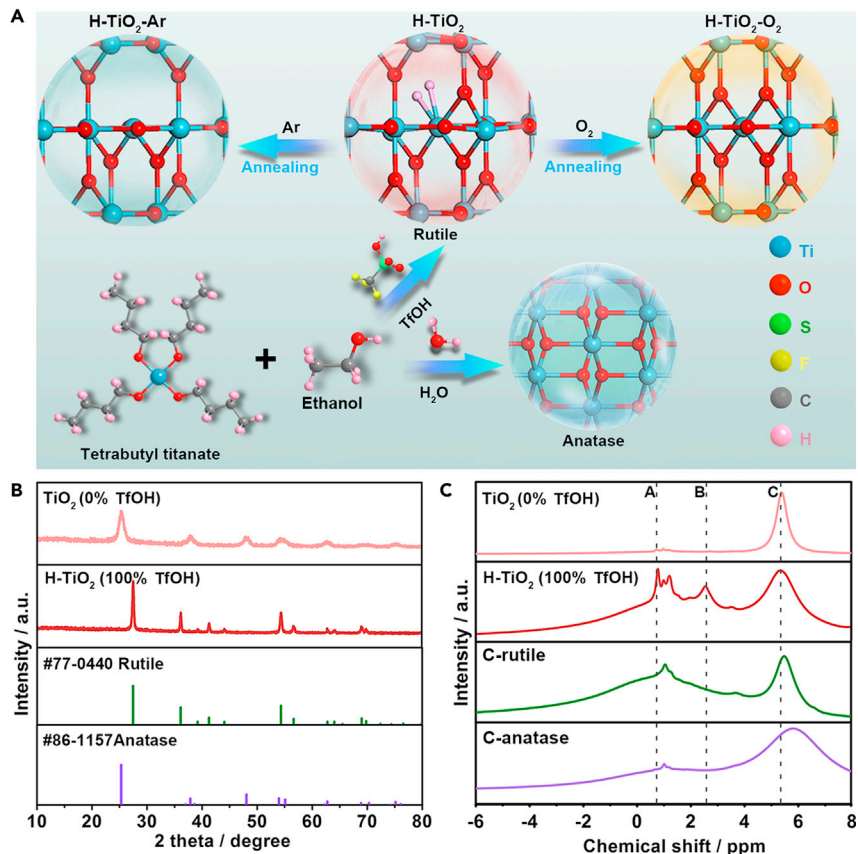


Figure 1. The synthesis and structural characterization of H-TiO₂

(A) Schematic illustration of the synthesis of H-TiO₂ in TfOH and the defect switch strategy: TiO₂ with or without oxygen vacancies could be separately obtained by annealing in Ar or O₂ atmospheres (products denoted as H-TiO₂-Ar or H-TiO₂-O₂, respectively).

(B) XRD patterns of TiO₂ (0% TfOH), H-TiO₂ (100% TfOH), and standard rutile and anatase PDF. (C) ¹H NMR spectra of TiO₂ (0% TfOH), H-TiO₂ (100% TfOH), C-rutile, and commercial anatase (C-anatase).

(Figure S10). The third stage is at 350 to 370°C due to small amounts of organic molecules lost on the surface of H-TiO₂ based on the mass spectra (Figure S11).³⁰ Interestingly, we find that the H-TiO₂ annealed under Ar and O₂ atmosphere shows different colors. As shown in Figure 2B, the as-prepared H-TiO₂ is slightly dark yellow, while the color of oxygen-treated H-TiO₂ is white. The Ar-treated H-TiO₂ transforms into pronounced black, indicating the appearance of Ti³⁺ species and oxygen vacancies in the hydrogenated TiO₂.² Ultraviolet-visible (UV-vis) spectra show that H-TiO₂ has a new absorption peak in the visible region (420–740 nm), and H-TiO₂-Ar has a redshift (480–760 nm) compared with the H-TiO₂-O₂ and H-TiO₂ (inset of Figure 2B).^{21,31} ¹H NMR spectra show that the peak of 0.78 ppm in H-TiO₂-O₂ and H-TiO₂-Ar disappears, suggesting Ti-H bonds are removed at the high temperature (Figure 2C). The solid FT-IR identifies the Ti-H species in H-TiO₂ before annealing (Figure S12).³² XRD spectra show that the main crystal structures of H-TiO₂-O₂ and H-TiO₂-Ar do not change during the annealing treatment compared with H-TiO₂ (Figures S13 and S14). This indicates that the hydrogen doping does not change the crystal structure. Raman spectra show that the E_g peaks of H-TiO₂ and H-TiO₂-Ar shift and broaden, indicating that the original symmetry of TiO₂ lattice is broken due to the oxygen vacancy in H-TiO₂-Ar and the Ti-H defect in

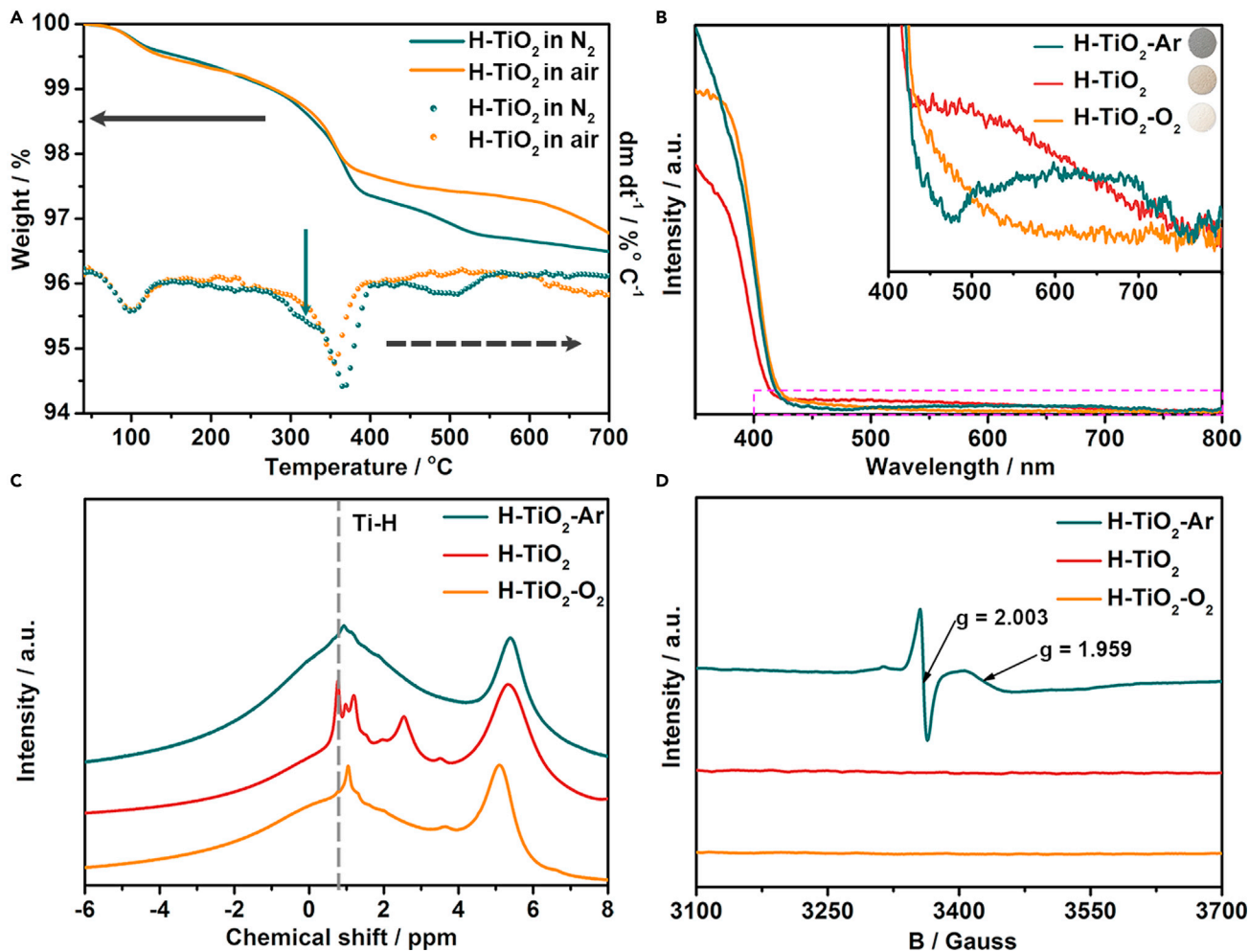


Figure 2. Characterization of switchable defects engineering

- (A) Thermogravimetric analysis of H-TiO₂ in N₂ and air atmosphere.
- (B) UV-vis spectra and photos (inset: enlarged pink rectangle region) of H-TiO₂, H-TiO₂-O₂, and H-TiO₂-Ar.
- (C) ¹H NMR spectra of H-TiO₂, H-TiO₂-O₂, and H-TiO₂-Ar.
- (D) EPR spectra of H-TiO₂, H-TiO₂-O₂, and H-TiO₂-Ar.

H-TiO₂ (Figure S15).²¹ Electron paramagnetic resonance (EPR), which is sensitive to unpaired electrons, is used to identify Ti³⁺ species and associated oxygen vacancies. H-TiO₂ shows no defect signals. However, the g-tensor of Ti³⁺ species (1.959) and associated oxygen vacancies (2.003) are observed for H-TiO₂-Ar and TiO₂-50%-Ar-500 (Figures 2D and S16), assigned to the trapped electron.^{21,33} The corresponding g-tensor signals disappeared after O₂ annealing treatment. The peaks corresponding to oxygen vacancies and Ti³⁺ become more prominent when the temperature is increased from 300 to 700°C in Ar (Figure S17).

Atomic scale structures are probed by aberration-corrected annular dark field scanning transmission electron microscopy (ADF-STEM). TEM images show that the diameters of H-TiO₂-O₂ and H-TiO₂-Ar nanorods are increased with the temperature (Figure S18). The morphology and diameter of H-TiO₂-O₂ at 700°C are similar to that of C-rutile (Figure S19). The specific surface area decreases with the increase of annealing temperature (Figure S20 and Table S1). ADF-STEM images in Figures 3A–3C show that the H-TiO₂-Ar product has clear lattice distortion compared with H-TiO₂.

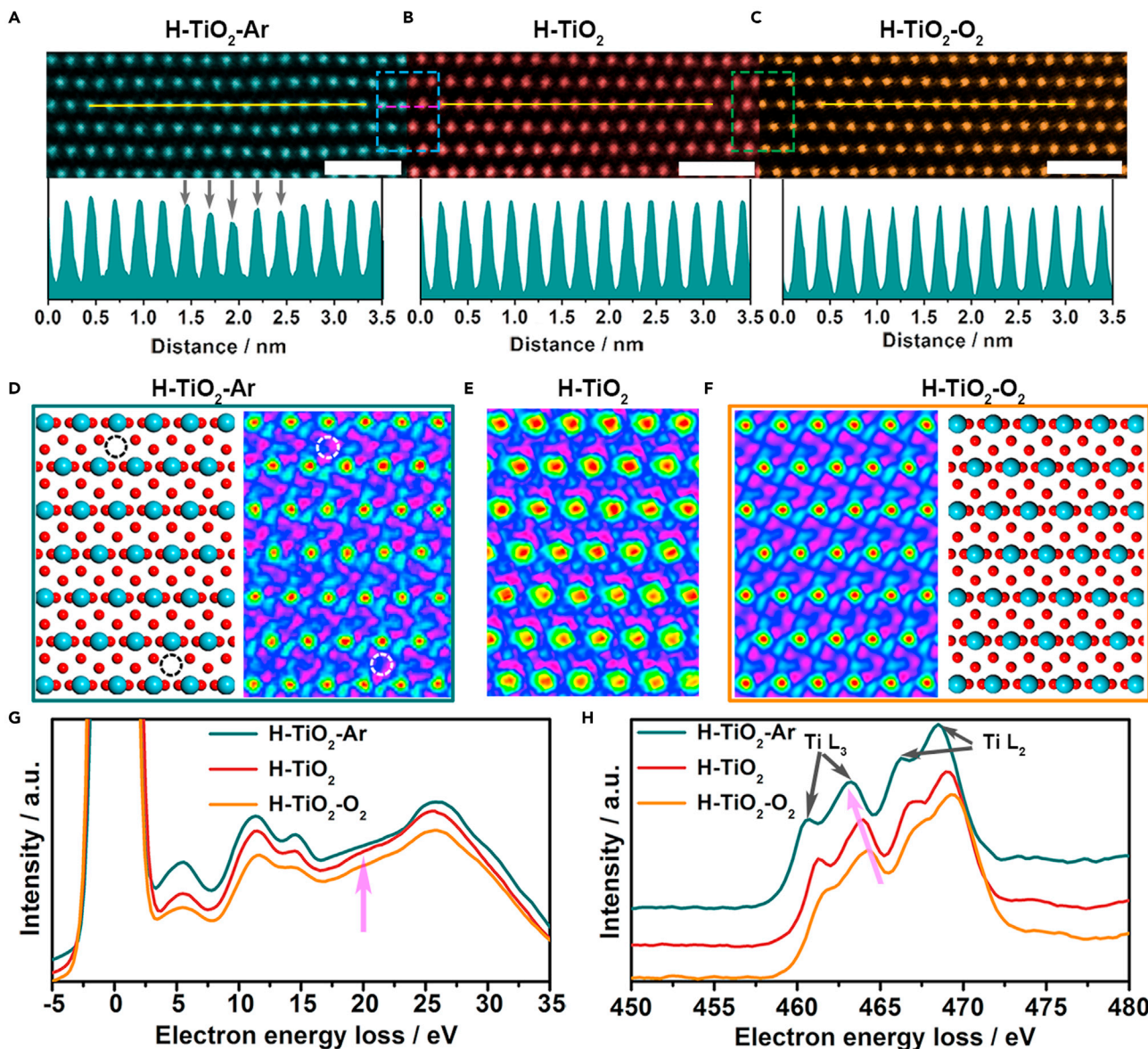


Figure 3. Atomic scale structure analysis of H-TiO₂-Ar, H-TiO₂, and H-TiO₂-O₂

(A–C) ADF-STEM images and corresponding intensity line profile extracted from the yellow line of ADF-STEM of H-TiO₂-Ar (A), H-TiO₂ (B), and H-TiO₂-O₂ (C), scale bar, 1 nm.

(D) Crystal structure of rutile TiO₂ along (1–11) zone axis and the enlarged rainbow-colored ABF-STEM images of H-TiO₂-Ar, black and white dotted circles represent the oxygen vacancies.

(E) Enlarged rainbow-colored ABF-STEM images of H-TiO₂.

(F) Rainbow-colored ABF-STEM images and the corresponding crystal structure of H-TiO₂-O₂.

(G and H) EELS spectra at low energy (G) and high energy (H) of H-TiO₂-Ar, H-TiO₂, and H-TiO₂-O₂.

and H-TiO₂-O₂ (Figures S21–S23). The distortion can be clearly observed in the corresponding intensity line profiles of the bottom panel (indicated by black arrows) of Figures 3A–3C. Slight displacements of Ti atoms were also observed, as indicated in dashed rectangles in the upper panel of Figures 3A–3C. We ascribe this lattice distortion to the existence of oxygen vacancies, observed by the enlarged rainbow-colored ABF-STEM images in H-TiO₂-Ar compared with H-TiO₂

and H-TiO₂-O₂ (dotted circle represents the oxygen vacancy, [Figures 3D–3F](#) and [S21–S23](#)). These results confirm the defects switch from the hydrogen doping to oxygen vacancies when H-TiO₂ is annealed under Ar, and the defects are repaired when H-TiO₂ is annealed under O₂.

Electron energy loss spectroscopy (EELS) is further conducted to obtain a qualitative interpretation of chemical bonding. As shown in [Figure 3G](#), H-TiO₂ presents a new peak at ~20 eV, which is similar to the Ti-H in TiH₂ at low energies.^{34,35} This peak disappears at high temperature for H-TiO₂-Ar and H-TiO₂-O₂. [Figure 3H](#) shows that the Ti L peaks at high energy (460–470 eV) of H-TiO₂-Ar shift to lower energies compared with H-TiO₂ and H-TiO₂-O₂. This indicates a reduced valence state of titanium and confirms the existence of oxygen defects. These phenomena imply that the hydrogen atoms inside the lattice are removed after high temperature treatment, resulting in the reduction of the surface of the sample.^{36,37}

The chemical states of different samples are investigated by X-ray photoelectron spectroscopy (XPS). As shown in [Figure 4A](#), H-TiO₂ shows Ti⁴⁺ peaks with binding energy of 458.3 eV and 464.1 eV and a well-formed O 1s peak at 530.0 eV belonging to the crystal lattice oxygen of H-TiO₂. H-TiO₂-O₂ shows an increase (0.2 eV) of binding energy of Ti⁴⁺ and a decrease (0.2 eV) of O 1s. This is due to the higher electronegativity of oxygen relative to hydrogen and is in good agreement with the pristine rutile TiO₂.³⁸ H-TiO₂-Ar exhibits an obvious Ti³⁺ chemical state at 456.9 eV and 462.5 eV and a higher binding shift of O 1s spectrum at 530.1 eV, indicating the appearance of oxygen vacancies.²¹ No detectable TfOH acid or nitrogen species remains on the surface of H-TiO₂ based on the XPS spectra of F 1s and S 2p and N 1s ([Figures S24](#) and [S25](#)).

X-ray absorption fine structure (XAFS) analysis gives further insight into the coordination environment. [Figure 4B](#) shows that the Ti K-edge X-ray absorption near-edge structure (XANES) spectra of different samples are similar, confirming the similar local structure environment. Ti pre-edge peaks (4,969.4 eV, 4,972.0 eV, and 4,975.1 eV, the pink curve in the inset of [Figure 4B](#)) represent the transition of 1s → 3d and 1s → hybridized p-d for the octahedral symmetry, the intensity of which for H-TiO₂ is slightly higher than that of C-rutile and H-TiO₂-O₂, indicating distorted local structures due to the existence of Ti-H.³⁹ However, a higher intensity of pre-edge peak appears on the H-TiO₂-Ar curve compared with H-TiO₂, indicating more distorted local structures after Ar annealing treatment. Compared with H-TiO₂, H-TiO₂-O₂, and C-rutile, the intensity of the white line (light green range, [Figure 4B](#)) decreased and the adsorption edge shifted to lower energy for H-TiO₂-Ar, suggesting a decreased Ti oxidation state. In combination with XPS, H-TiO₂-Ar has a lower Ti valence state due to the appearance of Ti³⁺. The Fourier transform of extended XAFS (FT-EXAFS) spectra show a main peak at 1.50 Å, ascribed to the Ti-O scattering path ([Figure 4C](#)). The intensity of this peak decreases in the order of C-rutile, H-TiO₂-O₂, H-TiO₂, and H-TiO₂-Ar, revealing a decreased O coordination number of the Ti center.⁴⁰ Based on the least-squares fitting EXAFS results at 1.50 Å, these coordination numbers are obtained as 5.2, 5.5, 5.8, and 6.0 for H-TiO₂-Ar, H-TiO₂, H-TiO₂-O₂, and C-rutile, respectively ([Figures S26](#) and [S27](#); [Table S2](#)). Ti L-edge spectra were also studied to obtain an insight of the local electronic configuration. As shown in [Figure 4D](#), compared with H-TiO₂-O₂ and C-rutile, the onset energy position of the Ti L-edge shifts to a low energy for H-TiO₂, empirically suggesting a lower Ti valence state, and the lower valence state appears after annealing in Ar ([Figure 4E](#), purple arrow).⁴¹ The Ti 3d band is crystal field split into t_{2g} and e_g. The corresponding peak intensities change depending on the local

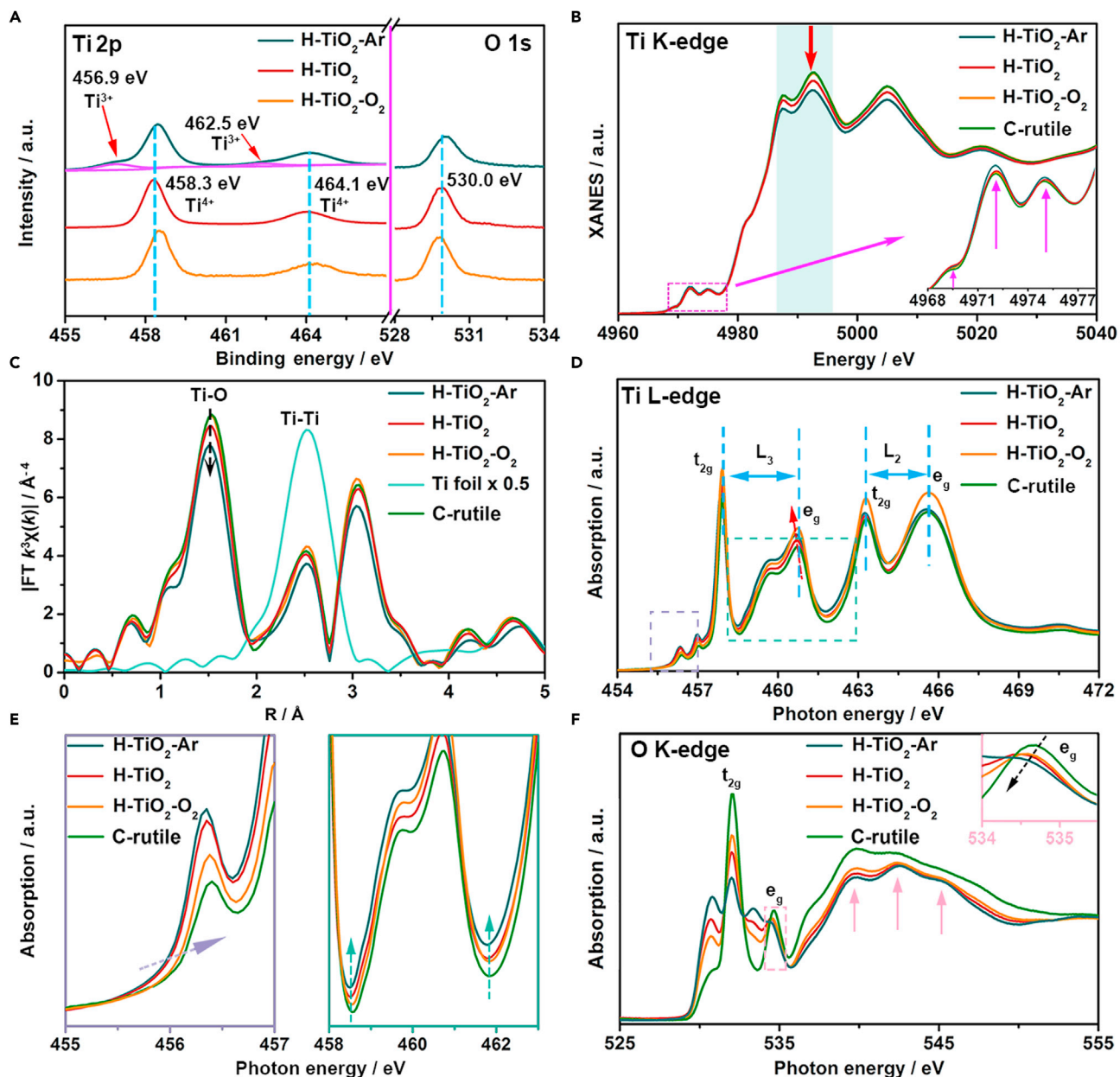


Figure 4. Local chemical environmental characterization of H-TiO₂, H-TiO₂-O₂, and H-TiO₂-Ar

(A) XPS spectra of Ti 2p and O 1s of H-TiO₂, H-TiO₂-O₂, and H-TiO₂-Ar.

(B–F) XANES spectra of Ti K-edge (B), k^3 -weighted FT-EXAFS spectra (C), Ti L-edge XAFS spectra (D), the enlarged XAFS spectra (E) of the dotted box in (D), and O K-edge XAS spectra (F) of H-TiO₂, H-TiO₂-O₂, H-TiO₂-Ar, and C-rutile.

structures. The Ti e_g band in particular is very susceptible to the local structure changes.^{42,43} A decrease in the crystal field, characterized by the separation between the t_{2g} and e_g peaks for H-TiO₂ and H-TiO₂-Ar is found compared with H-TiO₂-O₂ and C-rutile due to the lattice distortion after H incorporation and oxygen vacancy, respectively.⁴⁴ It is also noted that the reduced number of O around a Ti atom may reduce the O 2p – Ti 3d hybridization-induced crystal field. Furthermore, the slightly increased dips at 458.6 eV and 461.8 eV in the H-TiO₂ and H-TiO₂-Ar relative to H-TiO₂-O₂ and C-rutile (Figure 4E, green arrow) indicate a low Ti valence

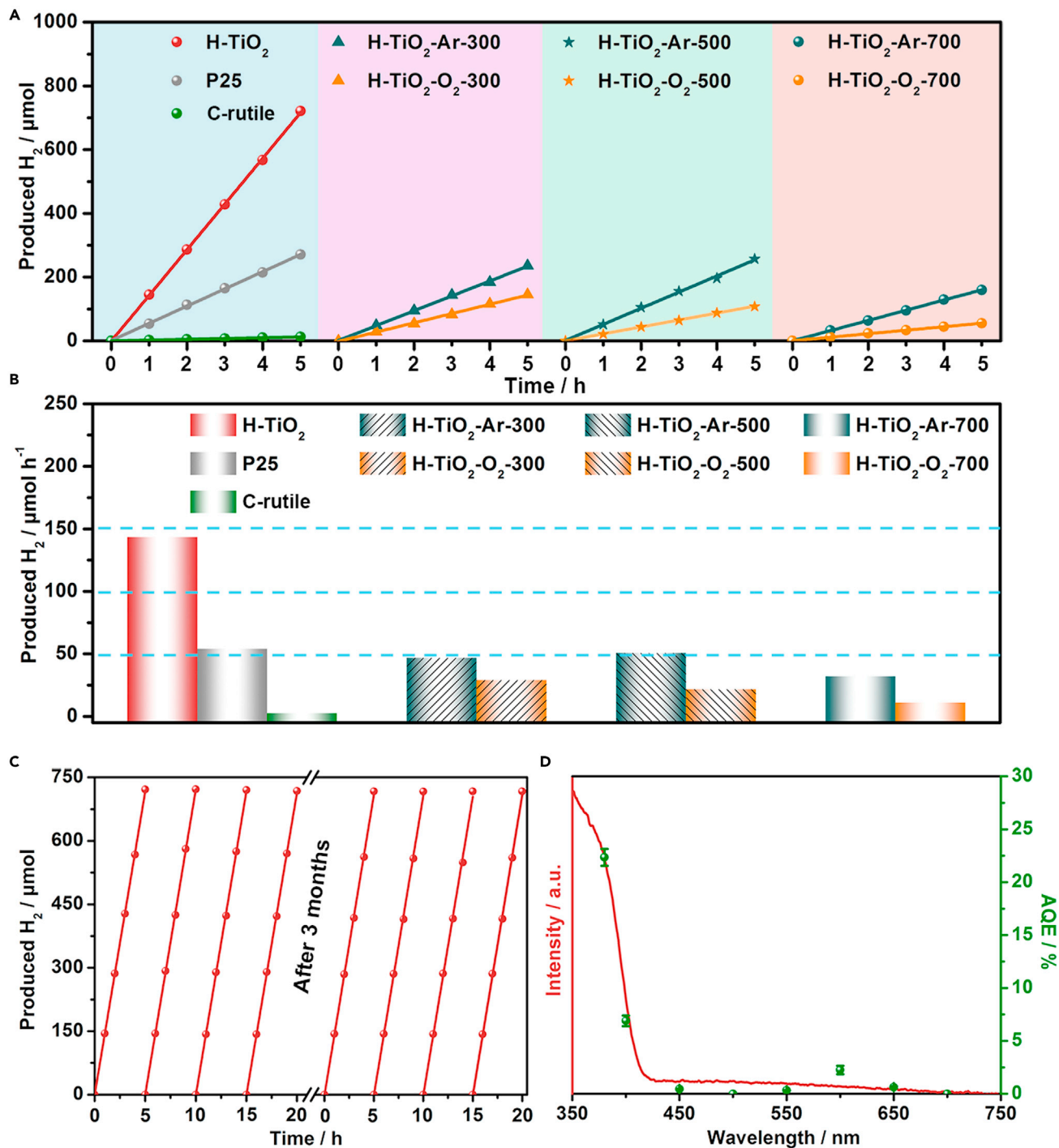
state in H-TiO₂ and H-TiO₂-Ar.^{45,46} O K-edge spectra were also obtained as shown in Figure 4F. The t_{2g} peaks for H-TiO₂ and H-TiO₂-Ar shift 0.2 eV to low energy compared with H-TiO₂-O₂ and C-rutile (the inset of Figure 4F), indicating slight variations in bond lengths.^{43,47,48} Also, three peaks at 539.8, 542.5, and 545.4 eV (Figure 4F, pink arrow) are considered as fingerprints of the rutile phase of TiO₂.⁴⁹

Photocatalytic hydrogen evolution performance

The photocatalytic hydrogen production performances were tested with Pt loading. The best photocatalytic hydrogen production rate was obtained at 1.78 wt% Pt (Table S3 and Figure S28). As shown in Figure 5A, the rates of photocatalytic hydrogen production for the samples increase linearly with the irradiation time. The photocatalytic hydrogen production efficiency of H-TiO₂ reaches a comparable hydrogen production rate of 142.9 $\mu\text{mol h}^{-1}$, which is 60 times that of C-rutile (2.4 $\mu\text{mol h}^{-1}$) and 2.7 times that of P25 nanoparticles (53.3 $\mu\text{mol h}^{-1}$) (Figure 5B; Video S1). The hydrogen evolution rate of H-TiO₂ is higher than that of the most reported literature data (Table S4). Furthermore, the hydrogen production rate was decreased after annealing in both Ar and O₂. The hydrogen evolution rate of H-TiO₂-Ar is higher than that of H-TiO₂-O₂ due to the presence of oxygen vacancy. Interestingly, in the visible light region, the hydrogen evolution rates of H-TiO₂ are 16 times that of P25. However, hydrogen production is not detected on C-rutile (Figure S29). Also, this H-TiO₂ shows that the activity is maintained at 99.4% after 3 months of storage and eight cycles, confirming the excellent photocatalytic stability (Figure 5C). There is no obvious change of the morphology and structure after the photocatalytic reaction (Figure S30). And no hydrogen escapes during the photocatalytic reaction and contributes to the produced H₂ under visible light (Figure S31). The control experiments (without light irradiation or photocatalysts) were also conducted and show no hydrogen evolution (Figure S32). Apparent quantum yield (AQY) was measured at different wavelengths (Figure 5D). The results indicate that the photocatalytic hydrogen evolution of H-TiO₂ is driven by photons.⁵⁰ H-TiO₂ shows the AQY of 22.3% (380 nm) and has excellent photocatalytic hydrogen evolution properties in the visible region with AQY of 2.2% at 600 nm. For comparison, we tested the photocatalytic properties of anatase TiO₂ obtained with concentration of 50% TfOH, and it also showed excellent hydrogen production property as compared with C-anatase, C-rutile, and annealed 50% TfOH anatase, but lower than that of H-TiO₂ (Figure S33). We also studied the photocatalytic hydrogen production properties in the absence of platinum co-catalyst. H-TiO₂ also shows the best photocatalytic performances (Figure S34).

Electronic structure

DFT calculations were used to investigate the effect of H incorporation in H-TiO₂. Total energy calculations and structure optimization show that replacing one oxygen atom with two hydrogen atoms is the most stable H-TiO₂ structure. The charge distribution for H-TiO₂ is shown in Figures 6A and S35. H-TiO₂ shows a stronger charge distribution asymmetry, which leads to the mismatch between the positive and negative charge centers than that of the pristine rutile TiO₂ due to Jahn-Teller effect, meaning the charge density for H-TiO₂ is redistributed after H incorporation. The introduction of hydrogen facilitates the charge separation in TiO₂, which is important to improve the photocatalytic hydrogen evolution activity. As shown in Figure 6B, the band structure shows that the introduction of H in H-TiO₂ does not change the pristine rutile bandgap of 3.00 eV. However, a new intermediate bandgap state does appear at 1.15 eV lower than the conduction band minimum. The density of states results in Figures 6C and 6D show new H-TiO₂ electron states near the Fermi level from hybridized orbitals of Ti, O, and H. This hybridized nature is

**Figure 5. Photocatalytic H₂ evolution performance evaluation**

(A) Time courses of photocatalytic H₂ evolution over H-TiO₂, commercial P25, C-rutile, and H-TiO₂-O₂ and H-TiO₂-Ar annealed at different temperatures of 300, 500, and 700°C under UV-vis irradiation (380–780 nm) with 20 vol% MeOH and 1.78 wt% Pt co-catalyst.

(B) H₂ generation activity values obtained from (A).

(C) Cycling test of H-TiO₂ under condition of (A).

(D) AQY of H-TiO₂ at different wavelengths with 20 vol% MeOH and 1.78 wt% Pt co-catalyst.

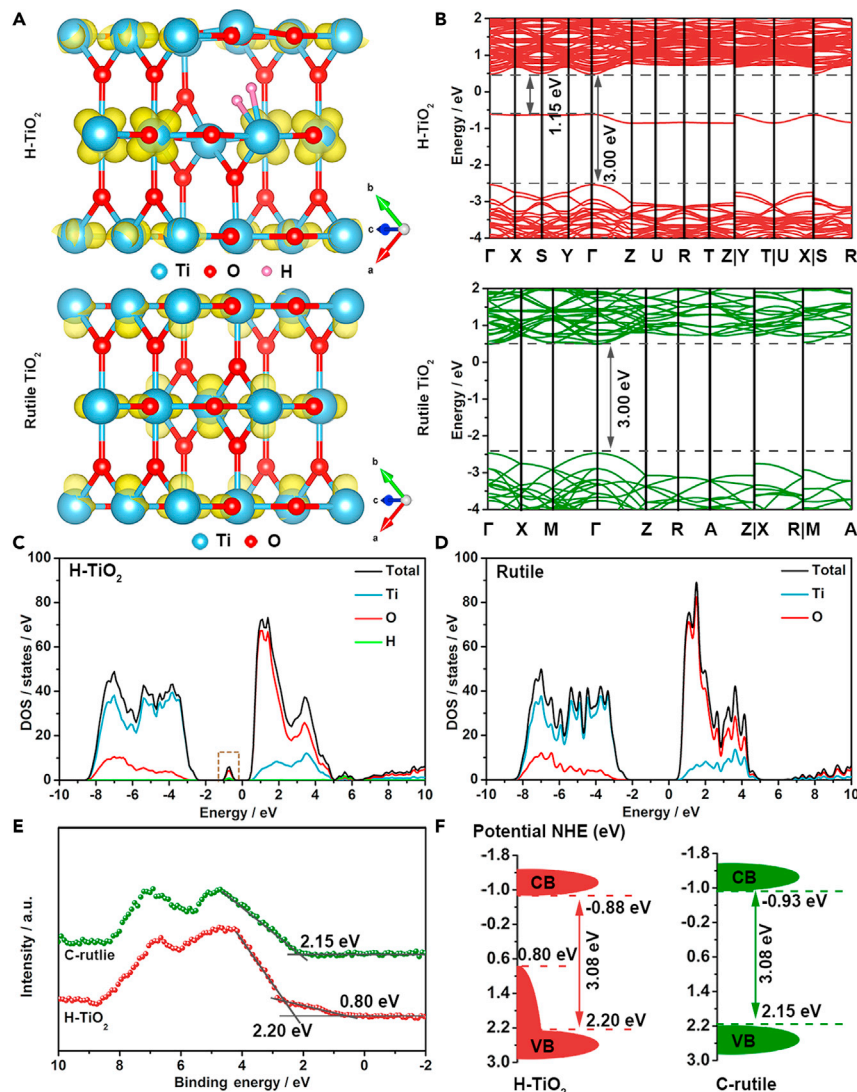


Figure 6. Electronic structure characterization

(A) Charge distribution of the bottom of conduction band of rutile TiO₂ and H-TiO₂ (the iso-density value: 0.004e Å⁻³).
(B–F) Band structure (B), calculated density of states (DOS) (C and D), VB-XPS (E), and band energy diagram (F) of C-rutile TiO₂ and H-TiO₂.

beneficial for the migration of photogenerated charges, suppressing the recombination of photogenerated electrons and holes compared with pristine rutile. These theoretical results were confirmed by the VB-XPS as shown in Figure 6E, in which H-TiO₂ shows an up-shift and a new tail of the valence band. As a result, the UV-vis spectra of H-TiO₂ show a new adsorption peak in the visible region (Figure S36A).¹⁵ Further, combining the VB-XPS and Tauc plot results (Figure S36B), the band energy diagram is proposed as shown in Figure 6F. Although the VB position (2.20 eV) and CB position (-0.88 eV) of H-TiO₂ is slightly down-shifted by 0.05 eV compared with pristine rutile, this tail (0.8 eV) of the VB top due to the presence of Ti-H bond for H-TiO₂ leads to extension of visible light absorption and transfer of photogenerated electron. Experimentally, photoluminescence spectra (PL) measurements were also conducted. The photoluminescence intensity of H-TiO₂

is lower than that of C-rutile under the same test conditions, indicating the fast carries separation (Figure S37). Accordingly, the electrochemical transient photocurrent test shows that the photocurrent response of the hydrogenated H-TiO₂ is better than that of P25 and C-rutile (Figure S38A). In addition, the electrochemical impedance also demonstrates that H-TiO₂ has an excellent photoelectron transfer capability (Figure S38B). We also calculated the hydrogen adsorption free energy on H-TiO₂. The results show that this energy on (110) facets of H-TiO₂ is lowered from the original -0.138 eV on rutile to 0.004 eV (Figure S39).⁵¹ This may also possibly contribute to the excellent photocatalyst activity of H-TiO₂ without platinum (Figure S34).

Conclusions

In conclusion, we achieve the synthesis of hydrogenated TiO₂ with Ti-H bond formed *in situ* by one pot wet-chemistry. The product shows high photocatalytic hydrogen evolution. We demonstrate that the introduction of hydrogen does not change the main crystal structure of TiO₂. Furthermore, this opens a path for controlled defect engineering of TiO₂ based on annealing environments. We achieve excellent hydrogen evolution rates of 142.9 μmol h⁻¹ under UV-vis, which is more than 60 times that of C-rutile. Characterization and theoretical calculations show that the improvement is due to the modified electronic structure and band structure for H-TiO₂. The demonstration of formation of metal-hydrogen bonds using wet-chemistry and the controllable defect engineering of metal oxides shows a great potential for adjusting the electronic structure of oxide semiconductors for the development of new photocatalysts.

EXPERIMENTAL PROCEDURES

Resource availability

Lead contact

Further information and requests for resources should be directed to and will be fulfilled by the Lead Contact, Xiaoqiang Cui (xqcui@jlu.edu.cn).

Materials availability

This study did not generate new unique reagents.

Data and code availability

This study did not generate any datasets.

SUPPLEMENTAL INFORMATION

Supplemental information can be found online at <https://doi.org/10.1016/j.matt.2021.10.027>.

ACKNOWLEDGMENTS

We thank the National Natural Science Foundation of China (12034002, 51872116, 52025025, and 52072400), the Natural Science Funds for Distinguished Young Scholar of Heilongjiang Province (No. JC2018004), the Excellent Young Foundation of Harbin Normal University (No. XKYQ201304), the Project for Self-innovation Capability Construction of Jilin Province Development and Reform Commission (2021C026), Jilin Province Science and Technology Development Program (20190201233JC), Program for JLU Science and Technology Innovative Research Team (JLUSTIRT, 2017TD-09), and the Fundamental Research Funds for the Central Universities. We thank the Beijing Synchrotron Radiation Facility (BSRF) and the Australian Synchrotron (VIC, Australia) for the XAS measurements.

AUTHOR CONTRIBUTIONS

X.C. directed this research. G.J. and Y.W. conducted most of the experiments. H.Z. and J.Z. performed the theoretical calculations. L.Z. and L.H.L. carried out the X-ray absorption experiments. Q.Z. and L.G. performed the TEM and HAADF-STEM characterization. Q.W., D.J.S., W.L., L.Z., J.W., and W.Z. contributed to data analysis. G.J., Y.W., and X.C. wrote the paper. X.C. and J.Z. supervised the project. G.J. and Y.W. contributed equally to this work. All authors discussed and reviewed the final manuscript.

DECLARATION OF INTERESTS

The authors declare no competing interests.

Received: January 24, 2021

Revised: March 4, 2021

Accepted: October 27, 2021

Published: November 16, 2021

REFERENCES

- Asahi, R., Morikawa, T., Ohwaki, T., Aoki, K., and Taga, Y. (2001). Visible-light photocatalysis in nitrogen-doped titanium oxides. *Science* 293, 269–271.
- Chen, X., Liu, L., Yu, P.Y., and Mao, S.S. (2011). Increasing solar absorption for photocatalysis with black hydrogenated titanium dioxide nanocrystals. *Science* 331, 746–750.
- Mali, S.S., Patil, J.V., Kim, H., and Hong, C.K. (2019). Gallium cationic incorporated compact TiO₂ as an efficient electron-transporting layer for stable perovskite solar cells. *Matter* 1, 452–464.
- Sun, X., Zhang, X., and Xie, Y. (2020). Surface defects in two-dimensional photocatalysts for efficient organic synthesis. *Matter* 2, 842–861.
- Wang, Z., Wen, B., Hao, Q., Liu, L.-M., Zhou, C., Mao, X., Lang, X., Yin, W.-J., Dai, D., Selloni, A., et al. (2015). Localized excitation of Ti³⁺ ions in the photoabsorption and photocatalytic activity of reduced rutile TiO₂. *J. Am. Chem. Soc.* 137, 9146–9152.
- Jia, G., Wang, Y., Cui, X., and Zheng, W. (2018). Highly carbon-doped TiO₂ derived from MXene boosting the photocatalytic hydrogen evolution. *ACS Sustain. Chem. Eng.* 6, 13480–13486.
- Melchionna, M., and Fornasiero, P. (2020). Updates on the roadmap for photocatalysis. *ACS Catal.* 10, 5493–5501.
- Scanlon, D.O., Dunnill, C.W., Buckeridge, J., Shevlin, S.A., Logsdail, A.J., Woodley, S.M., Catlow, C.R.A., Powell, M.J., Palgrave, R.G., Parkin, I.P., et al. (2013). Band alignment of rutile and anatase TiO₂. *Nat. Mater.* 12, 798–801.
- Wang, Z., Yang, C., Lin, T., Yin, H., Chen, P., Wan, D., Xu, F., Huang, F., Lin, J., Xie, X., et al. (2013). Visible-light photocatalytic, solar thermal and photoelectrochemical properties of aluminium-reduced black titania. *Energy Environ. Sci.* 6, 3007–3014.
- Zhang, Q., Lima, D.Q., Lee, I., Zaera, F., Chi, M., and Yin, Y. (2011). A highly active titanium dioxide based visible-light photocatalyst with nonmetal doping and plasmonic metal decoration. *Angew. Chem. Int. Ed.* 50, 7088–7092.
- Liu, G., Ma, L., Yin, L.-C., Wan, G., Zhu, H., Zhen, C., Yang, Y., Liang, Y., Tan, J., and Cheng, H.-M. (2018). Selective chemical epitaxial growth of TiO₂ islands on ferroelectric PbTiO₃ crystals to boost photocatalytic activity. *Joule* 2, 1095–1107.
- Moniz, S.J.A., Shevlin, S.A., Martin, D.J., Guo, Z.-X., and Tang, J. (2015). Visible-light driven heterojunction photocatalysts for water splitting—a critical review. *Energy Environ. Sci.* 8, 731–759.
- Kong, M., Li, Y., Chen, X., Tian, T., Fang, P., Zheng, F., and Zhao, X. (2011). Tuning the relative concentration ratio of bulk defects to surface defects in TiO₂ nanocrystals leads to high photocatalytic efficiency. *J. Am. Chem. Soc.* 133, 16414–16417.
- Ma, Y., Wang, X., Jia, Y., Chen, X., Han, H., and Li, C. (2014). Titanium dioxide-based nanomaterials for photocatalytic fuel generations. *Chem. Rev.* 114, 9987–10043.
- Naldoni, A., Allieta, M., Santangelo, S., Marelli, M., Fabbri, F., Cappelli, S., Bianchi, C.L., Psaro, R., and Dal Santo, V. (2012). Effect of nature and location of defects on bandgap narrowing in black TiO₂ nanoparticles. *J. Am. Chem. Soc.* 134, 7600–7603.
- Yang, Y., Yin, L.-C., Gong, Y., Niu, P., Wang, J.-Q., Gu, L., Chen, X., Liu, G., Wang, L., and Cheng, H.-M. (2018). An unusual strong visible-light absorption band in red anatase TiO₂ photocatalyst induced by atomic hydrogen-occupied oxygen vacancies. *Adv. Mater.* 30, 1704479.
- Liu, L., and Chen, X. (2014). Titanium dioxide nanomaterials: Self-structural modifications. *Chem. Rev.* 114, 9890–9918.
- Xie, L., Zhu, Q., Zhang, G., Ye, K., Zou, C., Prezdo, O.V., Wang, Z., Luo, Y., and Jiang, J. (2020). Tunable hydrogen doping of metal oxide semiconductors with acid-metal treatment at ambient conditions. *J. Am. Chem. Soc.* 142, 4136–4140.
- Selcuk, S., Zhao, X., and Selloni, A. (2018). Structural evolution of titanium dioxide during reduction in high-pressure hydrogen. *Nat. Mater.* 17, 923–928.
- Hu, Y.H. (2012). A highly efficient photocatalyst—hydrogenated black TiO₂ for the photocatalytic splitting of water. *Angew. Chem. Int. Ed.* 51, 12410–12412.
- Wang, Z., Yang, C., Lin, T., Yin, H., Chen, P., Wan, D., Xu, F., Huang, F., Lin, J., Xie, X., et al. (2013). H-doped black titania with very high solar absorption and excellent photocatalysis enhanced by localized surface plasmon resonance. *Adv. Funct. Mater.* 23, 5444–5450.
- Sinhamahapatra, A., Lee, H.-Y., Shen, S., Mao, S.S., and Yu, J.-S. (2018). H-doped TiO_{2-x} prepared with MgH₂ for highly efficient solar-driven hydrogen production. *Appl. Catal. B* 237, 613–621.
- Mao, H., Tang, J., Xu, J., Peng, Y., Chen, J., Wu, B., Jiang, Y., Hou, K., Chen, S., Wang, J., et al. (2020). Revealing molecular mechanisms in hierarchical nanoporous carbon via nuclear magnetic resonance. *Matter* 3, 2093–2107.
- Zhang, H., and Banfield, J.F. (2014). Structural characteristics and mechanical and thermodynamic properties of nanocrystalline TiO₂. *Chem. Rev.* 114, 9613–9644.
- Sabyrov, K., Burrows, N.D., and Penn, R.L. (2013). Size-dependent anatase to rutile phase transformation and particle growth. *Chem. Mater.* 25, 1408–1415.
- Yang, S., Hu, W., Zhang, X., He, P., Pattengale, B., Liu, C., Cendejas, M., Hermans, I., Zhang, X., Zhang, J., et al. (2018). 2D covalent organic frameworks as intrinsic photocatalysts for visible light-driven CO₂ reduction. *J. Am. Chem. Soc.* 140, 14614–14618.

27. Xu, F., Zhang, J., Zhu, B., Yu, J., and Xu, J. (2018). CuInS₂ sensitized TiO₂ hybrid nanofibers for improved photocatalytic CO₂ reduction. *Appl. Catal. B* 230, 194–202.
28. Donabauer, K., Maity, M., Berger, A.L., Huff, G.S., Crespi, S., and König, B. (2019). Photocatalytic carbaniion generation-benzylation of aliphatic aldehydes to secondary alcohols. *Chem. Sci.* 10, 5162–5166.
29. Manríquez, M.E., López, T., Gómez, R., and Navarrete, J. (2004). Preparation of TiO₂-ZrO₂ mixed oxides with controlled acid-basic properties. *J. Mol. Catal. A Chem.* 220, 229–237.
30. Li, L., Yan, J., Wang, T., Zhao, Z.-J., Zhang, J., Gong, J., and Guan, N. (2015). Sub-10 nm rutile titanium dioxide nanoparticles for efficient visible-light-driven photocatalytic hydrogen production. *Nat. Commun.* 6, 5881.
31. Zhang, K., Wang, L., Kim, J.K., Ma, M., Veerappan, G., Lee, C.-L., Kong, K.-j., Lee, H., and Park, J.H. (2016). An order/disorder/water junction system for highly efficient co-catalyst-free photocatalytic hydrogen generation. *Energy Environ. Sci.* 9, 499–503.
32. Yan, Y., Shi, W., Yuan, Z., He, S., Li, D., Meng, Q., Ji, H., Chen, C., Ma, W., and Zhao, J. (2017). The formation of Ti-H species at interface is lethal to the efficiency of TiO₂-based dye-sensitized devices. *J. Am. Chem. Soc.* 139, 2083–2089.
33. Naldoni, A., Altomare, M., Zopellaro, G., Liu, N., Kment, Š., Zbořil, R., and Schmuki, P. (2019). Photocatalysis with reduced TiO₂: from black TiO₂ to cocatalyst-free hydrogen production. *ACS Catal.* 9, 345–364.
34. Kihn, Y., Mirquet, C., and Calmels, L. (2005). EELS studies of Ti-bearing materials and ab initio calculations. *J. Electron Spectrosc. Relat. Phenom.* 143, 117–127.
35. Göpel, W., Anderson, J.A., Frankel, D., Jaehnig, M., Phillips, K., Schäfer, J.A., and Rocker, G. (1984). Surface defects of TiO₂(110): a combined XPS, XAES AND ELS study. *Surf. Sci.* 139, 333–346.
36. Lu, Y., Yin, W.-J., Peng, K.-L., Wang, K., Hu, Q., Selloni, A., Chen, F.-R., Liu, L.-M., and Sui, M.-L. (2018). Self-hydrogenated shell promoting photocatalytic H₂ evolution on anatase TiO₂. *Nat. Commun.* 9, 2752.
37. Guo, Y., Chen, S., Yu, Y., Tian, H., Zhao, Y., Ren, J.-C., Huang, C., Bian, H., Huang, M., An, L., et al. (2019). Hydrogen-location-sensitive modulation of the redox reactivity for oxygen-deficient TiO₂. *J. Am. Chem. Soc.* 141, 8407–8411.
38. Lu, X., Wang, G., Zhai, T., Yu, M., Gan, J., Tong, Y., and Li, Y. (2012). Hydrogenated TiO₂ nanotube arrays for supercapacitors. *Nano Lett.* 12, 1690–1696.
39. Cao, N., Chen, Z., Zang, K., Xu, J., Zhong, J., Luo, J., Xu, X., and Zheng, G. (2019). Doping strain induced bi-Ti³⁺ pairs for efficient N₂ activation and electrocatalytic fixation. *Nat. Commun.* 10, 2877.
40. Ma, R., Fukuda, K., Sasaki, T., Osada, M., and Bando, Y. (2005). Structural features of titanate nanotubes/nanobelts revealed by Raman, X-ray absorption fine structure and electron diffraction characterizations. *J. Phys. Chem. B* 109, 6210–6214.
41. Stoyanov, E., Langenhorst, F., and Steinle-Neumann, G. (2007). The effect of valence state and site geometry on Ti L_{3,2} and O K electron energy-loss spectra of Ti_xO_y phases. *Am. Mineral.* 92, 577–586.
42. Banerjee, D., Barman, A., Deshmukh, S., Saini, C.P., Maity, G., Pradhan, S.K., Gupta, M., Phase, D.M., Roy, S.S., and Kanjilal, A. (2018). Oxygen mediated phase transformation in room temperature grown TiO₂ thin films with enhanced photocatalytic activity. *Appl. Phys. Lett.* 113, 084103.
43. Kucheyev, S.O., van Buuren, T., Baumann, T.F., Satcher, J.H., Willey, T.M., Meulenbergh, R.W., Feiter, T.E., Poco, J.F., Gammon, S.A., and Terminello, L.J. (2004). Electronic structure of titania aerogels from soft x-ray absorption spectroscopy. *Phys. Rev. B* 69, 245102.
44. Zhang, Y., Li, L., Liu, Y., Feng, T., Xi, S., Wang, X., Xue, C., Qian, J., and Li, G. (2019). A symbiotic hetero-nanocomposite that stabilizes unprecedented CaCl₂-type TiO₂ for enhanced solar-driven hydrogen evolution reaction. *Chem. Sci.* 10, 8323–8330.
45. Chen, C., Avila, J., Frantzeskakis, E., Levy, A., and Asensio, M.C. (2015). Observation of a two-dimensional liquid of Fröhlich polarons at the bare SrTiO₃ surface. *Nat. Commun.* 6, 8585.
46. Park, Y., Sim, H., Jo, M., Kim, G.-Y., Yoon, D., Han, H., Kim, Y., Song, K., Lee, D., Choi, S.-Y., et al. (2020). Directional ionic transport across the oxide interface enables low-temperature epitaxy of rutile TiO₂. *Nat. Commun.* 11, 1401.
47. Al-Temimi, A., Prenger, K., Golnak, R., Loukasvuori, M., Naguib, M., and Petit, T. (2020). Impact of cation intercalation on the electronic structure of Ti₃C₂T_x MXenes in sulfuric acid. *ACS Appl. Mater. Interfaces* 12, 15087–15094.
48. Wang, Y., Jia, G., Cui, X., Zhao, X., Zhang, Q., Gu, L., Zheng, L., Li, L.H., Wu, Q., Singh, D.J., et al. (2021). Coordination number regulation of molybdenum single-atom nanzyme peroxidase-like specificity. *Chem* 7, 436–449.
49. Vásquez, G.C., Karazhanov, S.Z., Maestre, D., Cremades, A., Piqueras, J., and Foss, S.E. (2016). Oxygen vacancy related distortions in rutile TiO₂ nanoparticles: a combined experimental and theoretical study. *Phys. Rev. B* 94, 235209.
50. Wang, C., Wang, K., Feng, Y., Li, C., Zhou, X., Gan, L., Feng, Y., Zhou, H., Zhang, B., Qu, X., et al. (2021). Co and Pt dual-single-atoms with oxygen-coordinated Co-O-Pt dimer sites for ultrahigh photocatalytic hydrogen evolution efficiency. *Adv. Mater.* 33, 2003327.
51. Qi, K., Cui, X., Gu, L., Yu, S., Fan, X., Luo, M., Xu, S., Li, N., Zheng, L., Zhang, Q., et al. (2019). Single-atom cobalt array bound to distorted 1T MoS₂ with ensemble effect for hydrogen evolution catalysis. *Nat. Commun.* 10, 5231.